This paper is published as part of a *CrystEngComm* themed issue on:

Crystal Engineering in Molecular Magnetism

Guest Editors Concepció Rovira and Jaume Veciana
Institut de Ciència de Materials de Barcelona (ICMAB), Spain

Published in issue 10, 2009 of *CrystEngComm*

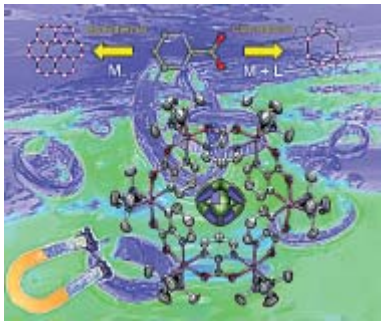

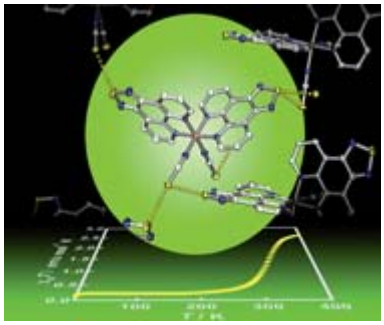

Images reproduced with permission of Enrique Colacio (left) and Kunio Awaga (right)

Papers published in this issue include:

Towards high T_c octacyanometalate-based networks
Barbara Sieklucka, Robert Podgajny, Dawid Pinkowicz, Beata Nowicka, Tomasz Korzeniak, Maria Bałanda, Tadeusz Wasiutyński, Robert Pełka, Magdalena Makarewicz, Mariusz Czapla, Michał Rams, Bartłomiej Gaweł and Wiesław Łasocha, *CrystEngComm*, 2009, DOI: 10.1039/b905912a

Cooperativity from electrostatic interactions: understanding bistability in molecular crystals
Gabriele D'Avino, Luca Grisanti, Anna Painelli, Judith Guasch, Imma Ratera and Jaume Veciana, *CrystEngComm*, 2009, DOI: 10.1039/b907184a

Anion encapsulation promoted by anion···π interactions in rationally designed hexanuclear antiferromagnetic wheels: synthesis, structure and magnetic properties
Enrique Colacio, Hakima Aouryaghal, Antonio J. Mota, Joan Cano, Reijo Sillanpää and A. Rodríguez-Diéguez, *CrystEngComm*, 2009, DOI: 10.1039/b906382j

Fe(II) spincrossover complex of [1,2,5]thiadiazolo[3,4-*f*][1,10]phenanthroline
Yoshiaki Shuku, Rie Suizu, Kunio Awaga and Osamu Sato, *CrystEngComm*, 2009, DOI: 10.1039/b906845g

Visit the *CrystEngComm* website for more cutting-edge crystal engineering research
www.rsc.org/crystengcomm

A new hybrid material exhibiting room temperature spin-crossover and ferromagnetic cluster-glass behavior†‡

Ana I. S. Neves, João C. Dias, Bruno J. C. Vieira, Isabel C. Santos, Moritz B. Castelo Branco, Laura C. J. Pereira, João C. Waerenborgh, Manuel Almeida, Dulce Belo* and Vasco da Gama*

Received 2nd April 2009, Accepted 26th June 2009
First published as an Advance Article on the web 24th July 2009
DOI: 10.1039/b906620a

A new compound, $[Fe(5–Cl-qsal)_2][Ni(\alpha\text{-tpdt})_2].CH_3CN$, where α-tpdt = 2,3-thiophenedithiolate and H5–Cl-qsal = N-(8-quinolyl)-5-chlorosalicylaldimine, was prepared and structurally and magnetically characterized. The crystal structure is based on an arrangement of alternate layers of $[Fe(5–Cl-qsal)_2]^+$ cations and $[Ni(\alpha\text{-tpdt})_2]^-$ anions. The magnetic measurements and Mössbauer spectroscopy revealed hybrid behavior in this compound, where a ferromagnetic cluster-glass behavior, ascribed to the anions network, and a spin crossover (SCO) of the $[Fe(5–Cl-qsal)_2]^+$ cations were observed. The glassy behavior, with a blocking temperature of *ca.* 7.5 K, results from the disorder in the anionic layer and the competition between ferro- and antiferromagnetic interactions in the anionic layers. The SCO process with $T_{1/2} = 298$ K (high spin fraction = $\gamma_{HS} = 0.5$) is rather sluggish in the limits of the conversion ($\gamma_{HS} \sim 0$ and $\gamma_{HS} \sim 1$), which is attributed to the effect of the anions that seem to restrict somehow the structural distortions of the cations associated with the SCO process.

Introduction

Spin crossover (SCO) compounds have attracted considerable interest in the last two decades and have been systematically studied due both to fundamental reasons and to their potential applications in devices.[1] More recently, a considerable attention was also devoted to the preparation of new SCO compounds, where the SCO properties are combined with other physical or chemical properties, such as magnetic networks, liquid crystalline properties, electrical conductivity, and non-linear optics, among others.[2]

Recently, our attention has been focused on developing transition metal complexes based on several new dithiothiophene ligands[3] that are expected to present a wide range of accessible oxidation states and favor solid state interactions. Among these, $[Ni(\alpha\text{-tpdt})_2]^-$ is a small planar paramagnetic $S = 1/2$ anion, that has already been used to prepare a variety of materials exhibiting interesting magnetic properties.[3a,4] Despite its relatively small size this anion exhibits a considerable spin density polarization over the ligand and as a consequence the magnetic interactions in these compounds are strongly dependent on the geometry of the intermolecular contacts. The crystal structures of the salts obtained so far with this anion depend on the cations, however they show a clear tendency to form layered arrangements, leading to an anion–cation segregation.

The crystal structures and magnetic behavior found in the $[Ni(\alpha\text{-tpdt})_2]^-$ based materials suggest that these anions are appropriate for obtaining hybrid molecular magnetic materials together with Fe^{III} SCO complexes, with ligands such as qsal derivatives, as these cationic complexes show also a strong tendency to form chains (and chain layers) due to π–π interactions between the ligands.[5] The complex $[Fe(qsal)_2]^+$ is a well known SCO system with relatively abrupt thermal interconversions between $S = 1/2$ and $S = 5/2$ states, depending on counterions and solvent presence. The same type of behavior is expected in complexes with qsal derivatives. In this paper we describe a hybrid system based on the SCO cation $[Fe(5–Cl-qsal)_2]^+$ and the paramagnetic anion $[Ni(\alpha\text{-tpdt})_2]^-$. The preparation of this hybrid material seems promising due to the combination of the SCO phenomena with the magnetic network of $[Ni(\alpha\text{-tpdt})_2]^-$. Furthermore the possible segregation from the two networks is expected to lead to strong cation–cation interactions and in this sense to a strong cooperative SCO process.

Results and discussion

Crystal structure of $[Fe(5–Cl-qsal)_2][Ni(\alpha\text{-tpdt})_2].CH_3CN$ (1)

The X-ray structure analysis of $[Fe(5–Cl-qsal)_2][Ni(\alpha\text{-tpdt})_2].CH_3CN$ (**1**), at 150 K, reveals that this compound

Dept. Química, Instituto Tecnológico e Nuclear/CFMCUL, P-2686-953 Sacavém, Portugal. E-mail: vascog@itn.pt; dbelo@itn.pt; Fax: +351219946185; Tel: +351219946203

† Electronic supplementary information (ESI) available: Tables of short contacts and hydrogen bonds in the crystal structure of $[Fe(5–Cl-qsal)_2][Ni(\alpha\text{-tpdt})_2].CH_3CN$ (Tables S1–S7 and Fig. S1–S8). CCDC reference numbers 725674 and 725675. For ESI and crystallographic data in CIF or other electronic format see DOI: 10.1039/b906620a

‡ **Crystallographic data for $(Fe(5–Cl-qsal)_2)[Ni(\alpha\text{-tpdt})_2].CH_3CN$ at 150 K**: $C_{42}H_{27}Cl_2FeN_5NiO_2S_6$, $M = 1011.51$ g mol^{-1}, triclinic, space group *P*-1, $a = 12.7394(13)$ Å, $b = 13.1194(10)$ Å, $c = 13.7931(14)$ Å, $\alpha = 108.043(3)°$, $\beta = 92.324(3)°$, $\gamma = 109.564(3)°$, $U = 2038.4(3)$ Å^3, $Z = 2$, $D_c = 1.648$ g cm^{-3}, μ(Mo Kα) = 1.302 mm^{-1}, 9942 reflections measured, 6560 unique, final $R(F^2) = 0.0596$ using 3902 reflections with $I > 2.0\sigma(I)$, R(all data) = 0.1218, $T = 150(2)$ K. CCDC725675.

Crystallographic data for $(Fe(5–Cl-qsal)_2)[Ni(\alpha\text{-tpdt})_2].CH_3CN$ at 294 K: $C_{42}H_{27}Cl_2FeN_5NiO_2S_6$, $M = 1011.51$ g mol^{-1}, triclinic, space group *P*-1, $a = 12.762(3)$ Å, $b = 13.148(3)$ Å, $c = 13.825(2)$ Å, $\alpha = 107.952(8)°$, $\beta = 92.416(8)°$, $\gamma = 109.564(8)°$, $U = 2051.9(7)$ Å^3, $Z = 2$, $D_c = 1.637$ g cm^{-3}, μ(Mo Kα) = 1.294 mm^{-1}, 12797 reflections measured, 7108 unique, final $R(F^2) = 0.0659$ using 3809 reflections with $I > 2.0\sigma(I)$, R(all data) = 0.1451, $T = 294(2)$ K. CCDC725674.

crystallizes in the triclinic space group *P*-1. The unit cell contains two independent $[Ni(\alpha\text{-tpdt})_2]^-$ anions (A1 and A2), placed in inversion centers and one independent $[Fe(5\text{–Cl-qsal})_2]^+$ cation (C), at general position.

The Ni–S bond distances, with an average value of 2.168 Å are typical of Ni^{III} dithiolates and the thiophenic ligand atomic bond lengths comparable to those previously reported for this anion.

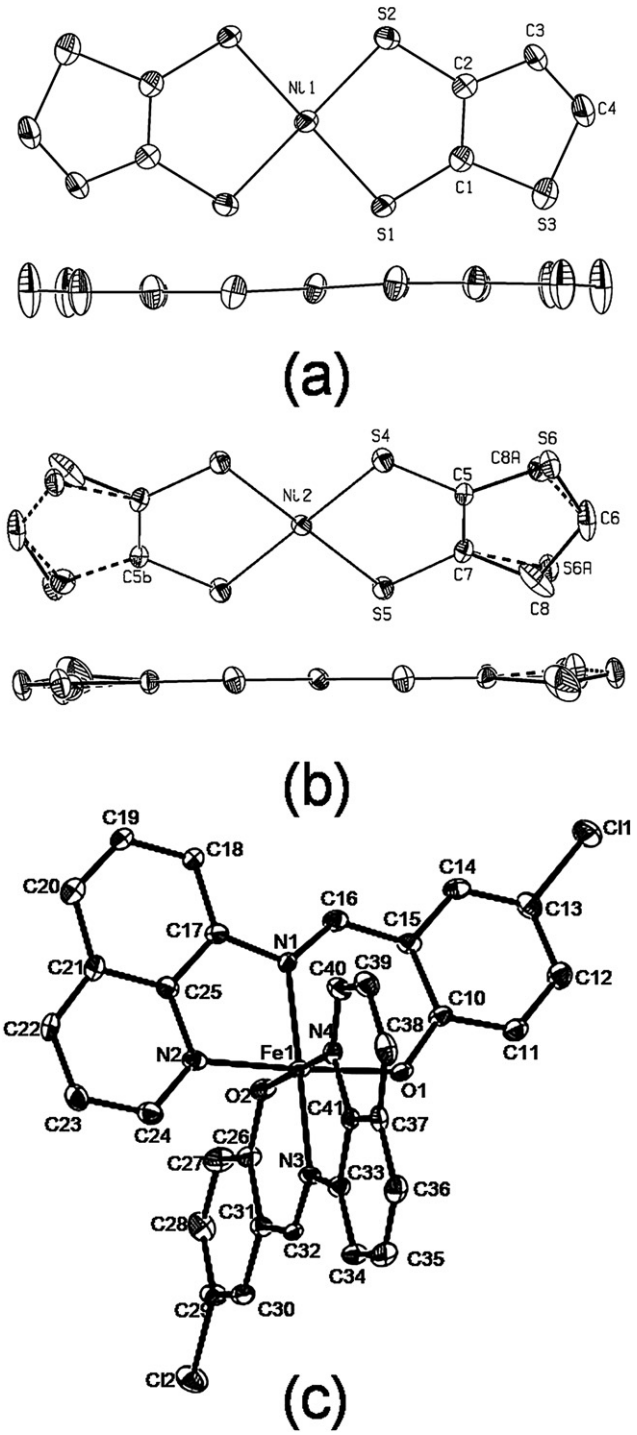

Fig. 1 ORTEP diagram at 40% probability level and atomic numbering scheme of $[Ni(\alpha\text{-tpdt})_2]^-$ as (a) A1 and (b) A2 and of (c) $[Fe(5\text{–Clqsal})_2]^+$ in the crystal structure of **1** (hydrogen atoms were omitted for clarity).

The $[Ni(\alpha\text{-tpdt})_2]^-$ anions are planar with the dithiothiophene ligands in a *trans* configuration. One of the $[Ni(\alpha\text{-tpdt})_2]^-$ species (A2) presents a disorder in the orientation of the thiophenic sulfur of the ligands, making it impossible to distinguish between a *cis* or *trans* conformation of the anion since both configurations, with orientation disorder in the crystal could give the observed results. This disorder could be modulated as resulting from a 57 : 43 occupation ratio of two positions involving atoms C8 and S6 (Fig. 1b). Since most of the $[Ni(\alpha\text{-tpdt})_2]^-$ anions previously reported, as well as A1 in this crystal structure, were found to crystallize in the *trans* configuration, the observed disorder is most likely a result of an orientational disorder of the complex in the *trans* configuration.

The iron atom is octahedrally coordinated by four nitrogen atoms and two oxygen atoms of two 5–Cl-qsal ligands, *i.e.*, an N_4O_2 donor set. The values of the bond lengths are consistent with those for typical LS Fe^{III} cations. The Fe–O distances (1.884(2) Å) are shorter than the Fe–N distances (1.957(1) Å), inducing a small distortion of the FeN_4O_2 octahedron. The two tridentate ligands in the cation are found to be nearly perpendicular to one another, adopting a *mer* configuration or an EF (edge-to-face) motif (bond angles between N4–Fe1–O2, N1–Fe1–N3 and O1–Fe1–N2 are, respectively, 176, 178 and 176°) (Fig. 1c).

The crystal structure consists of columns of cations surrounded by anionic layers and solvent molecules. The only short contact between cationic columns is along *b*, connecting a chlorine atom from one cation and a hydrogen atom from another, giving rise to a charge assisted hydrogen bond (Cl2···H38–C38). There are no short contacts between the anionic layers. Acetonitrile molecules, besides filling the empty spaces, behave like a bridge connecting cationic columns with each other, along *b*, and with anionic layers, along *c* (Fig. 2; see also ESI, Table S4†). These short contacts are mainly charge assisted hydrogen bonds between the acetonitrile nitrogen atom and hydrogen atoms from the cations and with the anion thiophenic sulfur atom and the methyl group from the solvent. In this sense the solvent molecules play and important and stabilizing role in this crystal packing.

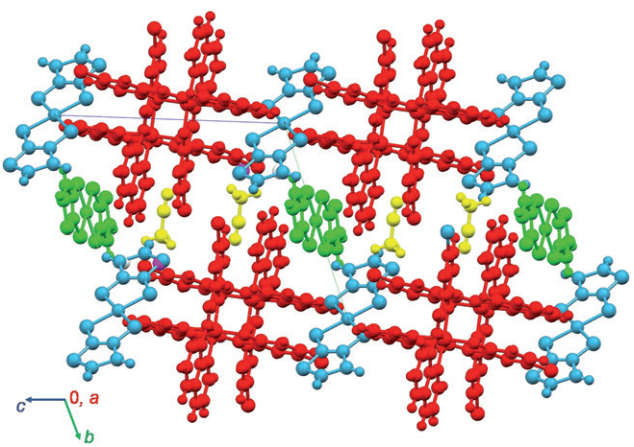

Fig. 2 (a) Crystal structure of **1**, viewed along *a* (cation: red, anion A1: green, anion A2: blue, CH_3CN: yellow).

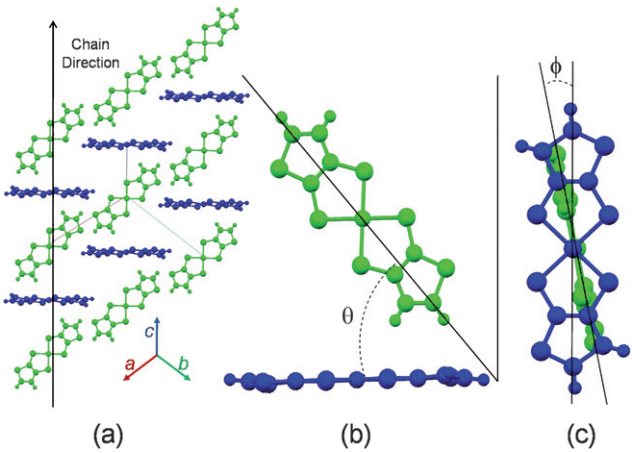

Fig. 3 Partial views of the crystal structure of **1** showing (a) one anionic layer; details showing anion contact modes (b) along c with $\theta = 49.9°$ and (c) along (1,1,1) with $\phi = 10°$. (A1: green and A2: blue).

The anionic layers are composed of zigzag chains of anions of the type A1A2A1A2, with the anionic molecular mean planes at an angle of 89° (Fig. 3). The anions within the chain are connected by hydrogen bonds involving the hydrogen atoms of one molecule (A1) and both the coordination and thiophenic sulfur atoms of the other (A2). Connecting these chains there is a $S_{thiophene}\cdots H$ hydrogen bond between neighboring A1 anions. Besides these short contacts, other interactions, both between and within chains, and slightly larger than the sum of the van der Walls radii, can be seen involving C···C and S···C atom pairs (Fig. 3; see also ESI, Table S5 and Fig. S1†).

The cation molecules stack in a similar fashion to the one previously described one for $[Fe(qsal)_2]^+$ compounds.[5] Along the stacks, the cations are related by an inversion center, in a OFF (offset face-to-face) chain motif, and kept tightly packed through several C···C short contacts, giving rise to a chain of π–π interactions, strengthened by O···H charge assisted hydrogen bonds (Fig. 2; see also ESI, Table S3 and Fig. S2†).

A large variety of anion–cation interactions are observed, contrasting with the absence of interactions between the anionic layers and the discrete interactions between cationic stacks (see ESI, Table S6†). Actually, the shapes of both the anion layers and the cation stacks seem to be very sensitive to the surrounding environment. Two types of cation–anion interactions were found. The first, involving A1 is mediated through a pair of short Ni···C short contacts and two S···H charge assisted hydrogen bonds, linking this anion to four cations, from two different stacks. The anion is placed almost parallel to one of the 5–Cl-qsal ligands, caging this molecule between two cations, from two different cationic stacks, and allowing significant π–π interactions between the cation ligand aromatic system and the anion carbon thiophenic ring atoms (Fig. 4a; see also ESI, Table S6, Table S7 and Fig. S3†). Probably these π–π interactions prevent the disorder in the thiophenic sulfur atom in A1. The cation–A2 interactions are independent of the sulfur thiophenic atom position. In this case the anion mean plane stays perpendicular to the cation ligands mean plane and the

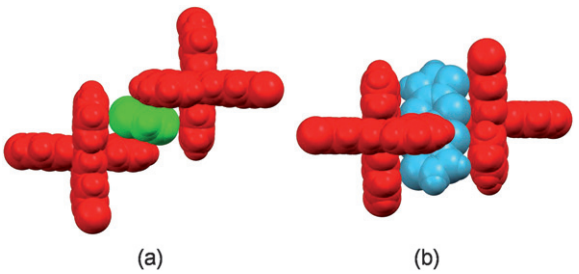

Fig. 4 Partial views of the crystal structure of **1** showing the cation–anion overlapping modes between (a) C(red)–A1(green) and (b) C(red)–A2(blue).

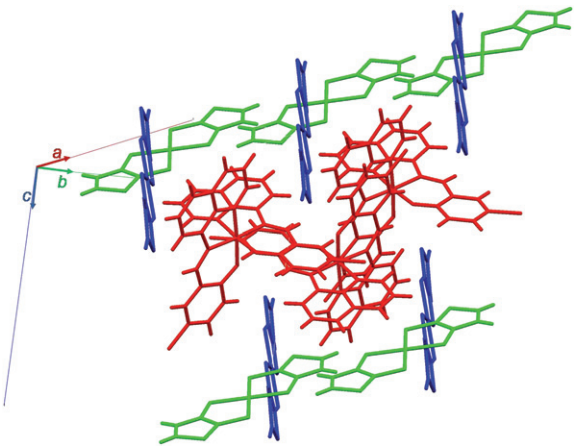

Fig. 5 Partial views of the crystal structure of **1** showing the locking between cation stacks and anionic layers (A1: green, A2: Blue, C: red. CH_3CN molecules were omitted for clarity).

observed interactions are S···H hydrogen bonds and a weak C···C short contact. Also, in this case A2 is surrounded by two pairs of cations from different stacks (Fig. 4b; see also ESI, Table S6 and Fig. S4†).

Altogether, these anion–cation-solvent interactions result in a good locking of the cationic stacks between the anion network and solvent molecules, constraining somehow the expected changes on the cation bond lengths associated with the SCO phenomena (see ESI, Table S6† and Fig. 5).

This is probably the reason why, comparing the crystal data obtained at 150 and at 294 K (see ESI†), we observe only a slight change on the Fe–N and Fe–O bond lengths. On the other hand, the crystal structure is flexibile enough to allow a subtle rearrangement of the anionic layers, by small variations of the cation "size".

An X-ray powder diffraction pattern was collected from the sample that was used in the Mössbauer spectroscopy and in the magnetic characterization. The obtained results are similar to the simulated powder diffraction pattern from the single crystal X-ray data (see ESI, Fig. S7†).

Mössbauer spectroscopy

The Mössbauer spectra of **1** obtained in the temperature range 4–295 K (Fig. 6) consist of four absorption lines which may be fitted with two quadrupole doublets. The estimated isomer shift,

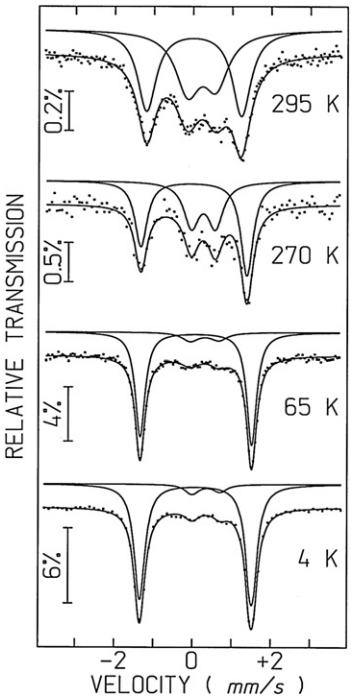

Fig. 6 Mössbauer spectra of **1** obtained at 4, 65, 270 and 295 K.

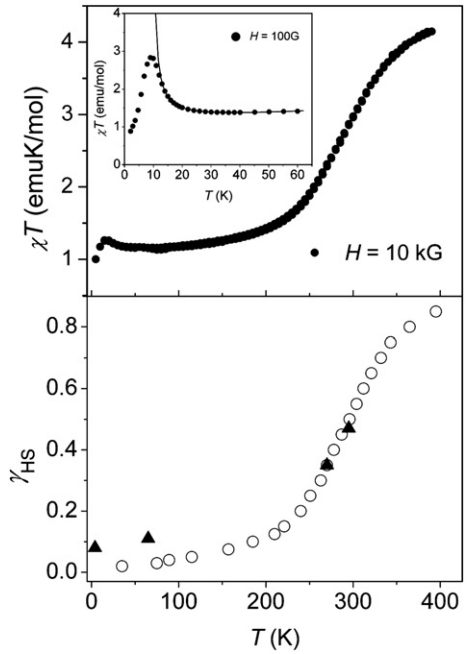

Fig. 7 χT temperature dependence of **1**; the inset shows the fit of the χT curve (100 G) at low temperatures (top). γ_{HS} temperature dependence obtained from the $\chi(T)$ data (open circles) and Mössbauer spectroscopy (triangles) (bottom).

Table 1 Estimated parameters from Mössbauer spectra of **1** taken at different temperatures[a]

	Fe^{III} spin	IS	QS	*W*	*I*
295 K	LS	0.13	2.42	0.36	53
	HS	0.33	0.73	0.38	47
270 K	LS	0.14	2.75	0.38	65
	HS	0.38	0.61	0.48	35
65 K	LS	0.20	2.85	0.30	89
	HS	0.42	0.72	0.51	11
4 K	LS	0.20	2.85	0.33	92
	HS	0.46	0.72	0.42	8

[a] LS low spin; HS high spin; IS (mm s^{-1}) isomer shift relative to metallic α-Fe at 300 K; *QS* (mm s^{-1}) quadrupole splitting; *W* (mm s^{-1}) line-width; *I* relative area. Estimated errors ≤ 0.02 mm s^{-1} for IS, QS, *W*, <3% for *I*.

IS, and quadrupole splitting, QS, are consistent with low spin, LS, (S = 1/2) and high spin, HS, (S = 5/2) Fe^{III} (Table 1). As usual for Fe^{III} the doublet with the lowest QS and highest IS is attributed to HS Fe^{III}. The doublet with the highest QS and the lowest IS is due to LS Fe^{III}.[6]

The coexistence of LS and HS Fe^{III} as well as the increase in the relative area, *I*, of HS Fe^{III} at 270 and 295 K, agree with magnetization data.

Magnetic properties

The temperature dependence of the χT product, where χ is the molar paramagnetic susceptibility (obtained with a 10 kG applied magnetic field), of **1** is shown in Fig. 7. At 390 K, $\chi T \sim 4.17$ emu K^{-1} mol^{-1} and upon cooling it decreases until $T \sim 100$ K. An inflection in the decrease is observed at ~ 300 K. Below 100 K, χT remains nearly constant ~ 1.15 emu K^{-1} mol^{-1}, with a broad minimum at ~ 60 K, then at *ca* 20 K it shows a maximum and decreases for lower temperatures. The high temperature decrease of χT is assigned to a spin crossover, SCO, process of the Fe^{III} cations, while the low temperature behavior is ascribed to a magnetic ordering phenomena in the anionic layers (described ahead).

The χT value at 390 K is lower than that expected for a system with the contributions of the anion (S = 1/2) and cation (S = 5/2) spins, 4.73 emu K^{-1} mol^{-1}, which indicates that at this temperature the SCO transition is not yet complete. After removing the magnetic contribution from the anions (see below), the calculated high spin fraction, γ_{HS}, at 390 K is approx. 0.85. From the $\chi(T)$ data it was possible to estimate the γ_{HS} temperature dependence (Fig. 7). A $T_{1/2}$ value of ~ 298 K for the SCO conversion ($\gamma_{HS} = 0.5$) was determined. Apart the contribution of a small HS impurity contamination, a reasonable agreement was observed between the γ_{HS} values obtained from the $\chi(T)$ data and the ones calculated from the Mössbauer spectroscopy. A sharper SCO process was anticipated as the π–π interactions between the 5–Cl-qsal ligands were expected to lead to a strong cooperativity between the SCO Fe^{III} centers, but as it is possible to see from the $\gamma_{HS}(T)$ curve, although this process is well defined in the $T_{1/2}$ region (250–350 K), it seems to be rather sluggish for $\gamma_{HS} < 0.2$ and for $\gamma_{HS} > 0.8$, corresponding to the beginning and the completion of the SCO transition. This behavior is attributed to the close packing arrangement around the $[Fe(5\text{–Cl-qsal})_2]^+$ chains by the anion network and solvent molecules, which seems to oppose the structural rearrangements associated with the SCO process.

At low temperatures ($15 < T < 60$ K), the behavior of $\chi(T)$ shows a good agreement with a model that considers the total

molar susceptibility as a sum of the independent contribution of the cationic and anionic networks, plus a term accounting for a relatively small HS impurity contribution: $\chi = \chi_C + \chi_A + \chi_{imp}$ (inset of the $\chi T(T)$ plot in Fig. 7). The cations were assumed to be LS and non-interacting, while the $S = 1/2$ anionic network shows significant anion–anion (AA) ferromagnetic (FM) interactions. A Curie–Weiss constant of 9.5 K, was obtained for χ_A. In this fit a g_A value of 2.06 [3a] was considered and the obtained value for $g_C = 2.3$ is in good agreement with the reported data for this type of Fe^{III} compounds.[5d,5f] The obtained χ_{imp} term was attributed to the presence of a contamination of ~6% of HS Fe^{III}, which is in reasonable agreement with the γ_{HS} value calculated from the Mössbauer spectra obtained at 4 K (see Table 1).

The McConnell I mechanism[7] has been widely used in the analysis of the intermolecular magnetic coupling in molecular crystals. According to this model the nature of the intermolecular coupling is determined by the spin density (SD) signs combination of the atoms involved in the shorter intermolecular contacts. An antiferromagnetic (AF) coupling is predicted when both atoms involved in the contact present the same SD sign and a FM coupling is expected in case of different signs. The $[Ni(\alpha\text{-tpdt})_2]^-$ anion is known to present a spin polarization effect,[4a] where one C and the S atoms from the thiophenic fragment of the α-tpdt ligand present negative SD values.

Within the anionic layers, based on arrangements of zigzag chains of anions, A1A2A1A2, several short contacts (slightly larger than the sum of the van der Waals radii) were found. The analysis of the AA contacts indicates that there is a coexistence of FM and AF AA interactions. The stronger intra- and interchain AA contacts (shorter contacts, involving atoms with larger SD) are illustrated in Fig. 8 where three anions are shown, A1 and A2 belonging to one chain and A1′ to an adjacent chain. The lighter atoms have positive SD, while the darker ones negative SD signs. The intrachain interactions are expected to be dominant and FM intrachain coupling is foreseen, as the atoms involved in those contacts show positive/negative SD. This is consistent with the positive θ value obtained from the $\chi(T)$ behavior at low temperatures. The interchain AA contacts are expected to lead to weaker AF interactions (larger intermolecular separations). The analysis of the variation of the intermolecular packing with temperature (see ESI, Fig. S1 and S6) indicates that the dominant intra- (A1–A2) and interchain (A2–A1′) AA interactions must become stronger with cooling (a detailed description of the intra- and interchain AA contacts is shown as ESI in Table S5 and Fig. S5 and S6†).

One of the $[Ni(\alpha\text{-tpdt})_2]^-$ anions (A2) presents a disorder in the orientation of the thiophenic S atom of the ligands. This disorder is not expected to induce major differences in the nature of the magnetic coupling. However, in the case of intrachain interactions, the predominant *trans* configuration is expected to lead to stronger intrachain FM interactions since these AA contacts are shorter. A considerable magnetic anisotropy is expected in the anionic layers composed by the weakly AF coupled FM chains. The disorder in the intrachain arrangements as well as the weak AF interchain coupling seem to play a crucial role in a low temperature magnetic ordering process described further down.

The low temperature behavior was examined in detail through low field dc magnetization measurements (obtained after cooling with different fields, M^{FC}, or in absence of an applied magnetic field, M^{ZFC}). These measurements suggest the existence of a magnetic ordering process at ~ 7.5 K, as indicated by the behavior of M^{FC}, M^{ZFC} and the remnant magnetization, M^{REM}, (with an applied magnetic field of 100 G) shown in Fig. 9. M^{FC} increases with cooling with a shoulder at ~7.5 K. For $T > 7.5$ K M^{ZFC} shows a similar behavior, but at the blocking temperature, $T_b = 7.5$ K, it diverges from the M^{FC} curve showing a maximum. With further cooling M^{ZFC} exhibits a minimum at ~5 K, then increases again for lower temperatures. M^{REM} starts to deviate from zero at ~12 K, which seems to correspond to the onset of a magnetically ordered regime occurring at ~7.5 K. The observed increase in M^{ZFC} for $T < 4$ K is consistent with the contribution of the Fe^{III} paramagnetic cations. The M^{FC} and M^{ZFC} results obtained at lower applied magnetic fields show an increase in the intensity of the peak at 7.5 K, while for higher fields the intensity decreases and eventually seems to fade away. T_b was also observed to decrease with the increase of the applied field (the $M/H(T)$ curves are shown as ESI, Fig. S8†). In order to achieve a better understanding of the magnetic ordering process, a variety of measurements, including magnetization isothermals and magnetic relaxation studies were performed.

The magnetization isothermals obtained at 2, 5 and 8 K (Fig. 10) show the experimental results increasing (solid symbols)

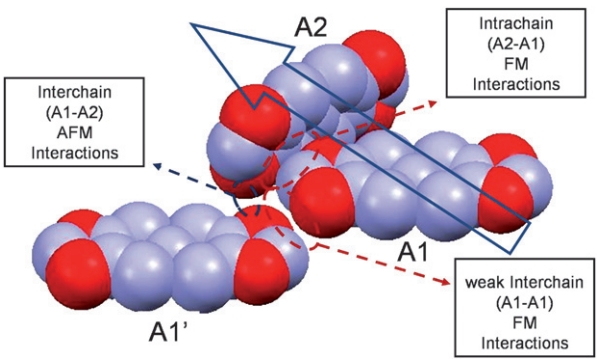

Fig. 8 Intra- (A1–A2) and interchain (A1–A1′ and A2–A1′) AA contacts in the $[Ni(\alpha\text{-tpdt})_2]^-$ anionic layers of **1**. Lighter atoms have positive SD and the darker ones negative SD.

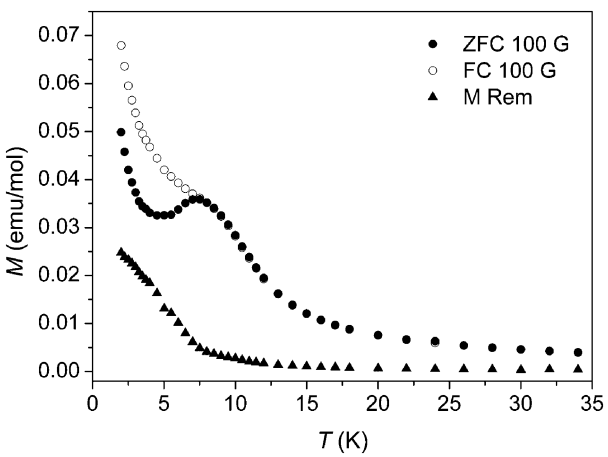

Fig. 9 M^{FC} M^{ZFC} and M^{REM}, temperature dependence (with $H = 100$ G) in **1**.

and decreasing (open symbols) the applied magnetic field. The solid curves in the plots correspond to the calculated Brillouin functions, with $S_C = S_A = 1/2$ and $g_A = 2.06$ and $g_C = 2.4$. From the isothermals it is possible to see that at 8 K, just before the magnetic ordering takes place, the magnetization data are larger than the calculated values for the Brillouin function, M_{Bf}, indicating the predominance of the FM interactions, in agreement with the observed results at higher temperatures. However, at low temperatures, the weaker AF interactions seem to play a crucial role in the magnetically ordered regime, at 5 K $M(H)$ is larger than $M_{Bf}(H)$ only up to ~20 kG and at 2 K $M(H)$ exceeds $M_{Bf}(H)$ only up to 3 kG. For that temperature, at high magnetic fields M_{Bf} is considerably larger than the measured magnetization. The insets of Fig. 10 show in detail the isothermals at low applied magnetic fields. The results at 2 and 5 K show a significant hysteresis, of ~350 and 50 G, respectively, and the remnant magnetization values of 100 and 11 emu mol^{-1} at 2 and 5 K, respectively. No hysteresis was detected at 8 K (just above T_b). At this temperature the dominance, in the range −500–500 G, $M(H)$ exceeds $M_{Bf}(H)$ by a factor of ~ 2–3.

A significant frequency dependence was observed in the real and imaginary components of the ac susceptibility (χ' and χ'', respectively), indicating that the magnetic ordering process does not correspond to long range ordering, but most likely to a short range order freezing process. The temperature dependencies of χ' and χ'' (with a 0 dc field and a 1 G ac field) at 99, 330, 990, 3330 and 9990 Hz, are shown in Fig. 11. $\chi'(T)$ exhibits a behavior closely resembling the one from $M^{ZFC}(T)$ at low applied magnetic fields. Besides the frequency dependence of the maxima at the freezing temperature, T_f, close to T_b, a clear increase is also observed at low temperatures. For both $\chi'(T)$ and $\chi''(T)$ the temperature of the maxima decreases as the frequency decreases. However, the intensity of the $\chi'(T)$ peak increases with decrease of the frequency, while the intensity of the $\chi''(T)$ peak decreases.

The frequency dependence of the ac susceptibility peaks is used to characterize the dynamic behavior of the freezing process through the empirical parameter $\phi = (\Delta T_f/T_f)/\Delta(\log(\nu))$, representing the relative shift of the freezing temperature, T_f, per frequency decade and a ϕ value of the order of 0.05 was obtained

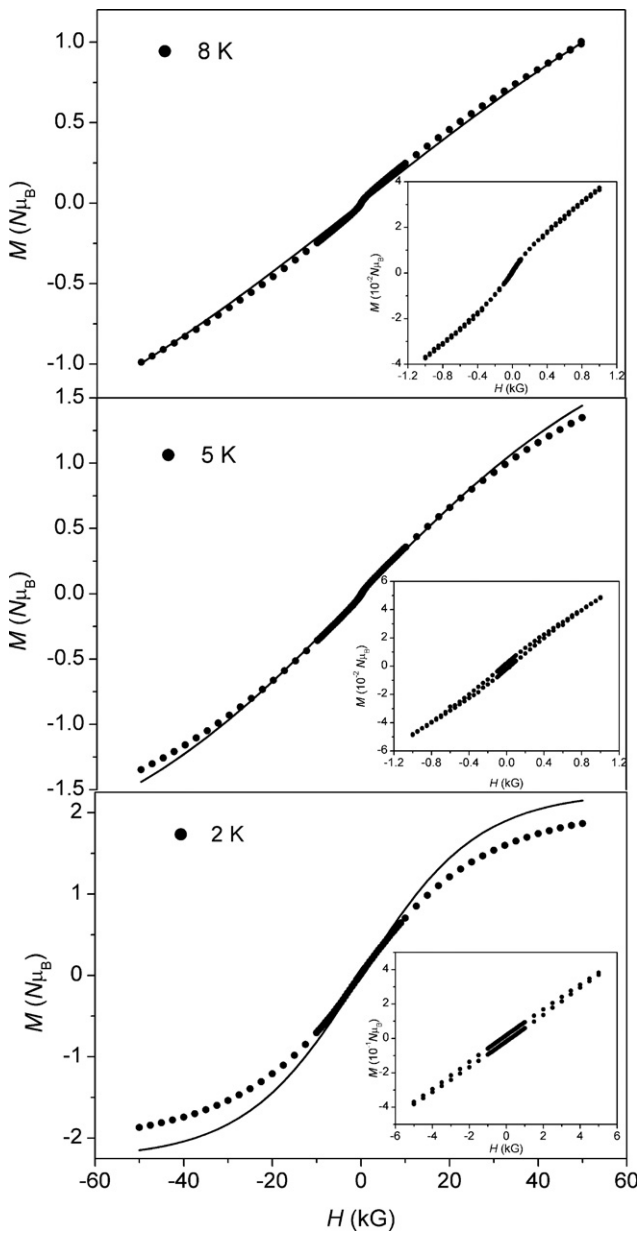

Fig. 10 Magnetization isothermals obtained at 8 (top), 5 (center) and 2 K (bottom) for **1**. The solid lines represent the calculated Brillouin functions for those temperatures. Details of the hysteresis loops are shown in the insets.

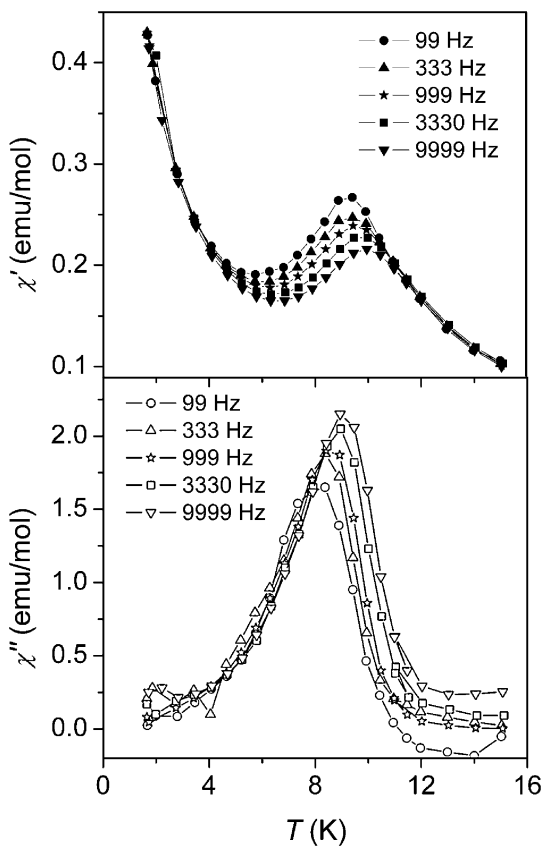

Fig. 11 Observed χ' (top) and χ'' (bottom) temperature dependencies at 99, 330, 990, 3330 and 9990 Hz for **1**.

from the peak positions in $\chi'(T)$ and $\chi''(T)$, which is consistent with a cluster-glass behavior.[8]

The relaxation time $\tau(T)$ temperature dependence, obtained from the $\chi'(T_f)$ maxima at a given frequency ($1/\tau = 2\pi\nu$), follows quite well the empirical Vogel–Fulcher law:[8] $\tau = \tau_0 \exp[E_a/k_B(T_f\text{-}T_0)]$, where τ_0 is the characteristic relaxation time, E_a is the activation energy (k_B is the Boltzmann constant) and T_0 is a parameter that accounts for the intercluster interactions. The best fit to the experimental results yields $\tau_0 = 7.97 \times 10^{-12}$ s, $E_a/k_B = 42.0$ K and $T_0 = 7.05$ K. The obtained magnetization relaxation time, τ_0, lies in the range 10^{-6} to 10^{-13}s typical of cluster-glass systems.[9] These results are consistent with the existence of strong inter-cluster interactions, as the parameter T_0 presents a value close to the observed freezing temperatures.[10]

The magnetization relaxation for the thermoremanent (TRM) mode was also probed following the decay of the magnetization, after field cooling and removing an applied field of 5 KG, for periods of approximately 4 h. Fig. 12 shows TRM measurements for temperatures below T_b, 2, 4 and 7 K. The 2 and 4 K curves could be fitted with a stretched exponential as $M(t) = M_0 + \sigma_0 e^{-(t/\tau)1-n}$, where M_0, and σ_0 are related with the FM and glassy components, respectively. τ is the time constant and n is related to the relaxation time. The best fit was obtained with $\tau = 2.1 \times 10^5$ and 2.5×10^4 s, for 2 and 4 K, respectively. The values of n are 0.66 and 0.29 at 2 and 4 K, respectively. M_0 was also required for these fits and found positive, 0.06 and 0.02 emu mol^{-1} for 2 and 4 K, respectively. The obtained fitting parameters are in good agreement with the experimental data and indicative of the already expected coexistence of FM and glassy magnetic components in the relaxation process. This type of behavior was also reported for manganites, perovskites and intermetallics.[11] Unlike those data, the measurements obtained at 7 K could not be adjusted to the stretched exponential behavior, suggesting the existence of a negative residual magnetization ($M_0 < 0$) but they failed to indicate any magnetization relaxation, which seems to agree with the anomaly expected to occur at $T = T_0 \sim 7$ K, according to the ac susceptibility relaxation results.

The magnetic data and the intermolecular coupling analysis clearly indicate a cluster-glass behavior that can be assigned to the existence of AF interacting FM domains. With cooling small 2D regions consisting in arrangements of FM chain fragments, from the anionic chains are expected to form and freeze at low temperatures ~7 K. The weaker intrachain FM interaction associated with the presence of anions in the minority *cis* conformation combined with the disorder induced by the thermal energy, is expected to lead to the fragmentation of the FM chains. With cooling, these chain fragments must give rise to FM domains that interact between themselves through the AF interchain coupling described above.

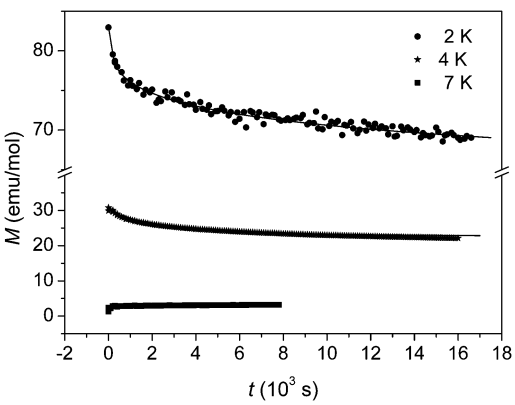

Fig. 12 Magnetization relaxation at 2, 4 and 7 K for **1**.

Experimental

General materials and methods

All manipulations were carried out under strict anaerobic conditions under dry nitrogen or argon atmosphere unless stated otherwise. All solvents were dried and purified following standard procedures. n-$Bu_4N[Ni(\alpha\text{-tpdt})_2]$[3a] and $[Fe(5\text{–Cl-qsal})_2]BF_4$[12] were synthesised as previously described. Other chemicals were commercially obtained and used without any further purification. Melting points were measured with a Stuart Melting Point Apparatus SMP3, with a maximum temperature of 310 °C.

Synthesis of the complex

$[Fe(5\text{–Cl-qsal})_2][Ni(\alpha\text{-tpdt})_2].CH_3CN$ (1). A solution of $[Fe(5\text{–Cl-qsal})_2]BF_4$ (141 mg, 0.2 mmol) in CH_3CN (*ca.* 20 ml) was added dropwise to a solution of n-$Bu_4N[Ni(\alpha\text{-tpdt})_2]$ (119 mg, 0.2 mmol) also in CH_3CN (*ca.* 20 ml). A dark-green precipitate was filtered affording suitable crystals for X-ray diffraction. Yield 30% (0.061 g) mp > 310 °C. CHNS ($C_{42}H_{27}Cl_2FeN_5NiO_2S_6$): calc. C 49.87, H 2.69, N 6.92, S 19.11; found C 48.37, H 3.57, N 6.30, S 20.00.

X-Ray crystallography

X-Ray diffraction experiments were performed with a Bruker AXS APEX CCD detector diffractometer using graphite monochromated Mo Kα radiation ($\lambda = 0.71073$ Å), in the φ and ω scans mode. A semiempirical absorption correction was carried out using SADABS.[13] Data collection, cell refinement and data reduction were done with the SMART and SAINT programs.[14] The structures were solved by direct methods using SIR97[15] and refined by full-matrix least-squares methods using the program SHELXL97[16] and the winGX software package.[17] Non-hydrogen atoms were refined with anisotropic thermal parameters, whereas H-atoms were placed in idealized positions and allowed to refine riding on the parent C atom. Molecular graphics were prepared using ORTEP 3.[18] X-Ray powder diffraction patterns were taken at room temperature using a Philips X′pert diffractometer (Bragg–Brentano assembly, monochromated Cu Ka radiation, $5 < 2\theta < 30°$, step with 0.01°, and 20 s of couting time per step). The collected powder data were compared to the simulated powder diffraction pattern from the single crystal X-ray data using the program PowderCell.[19]

Mössbauer spectroscopy

Mössbauer spectra were collected in the 4–295 K temperature range, in transmission mode, using a conventional

constant-acceleration spectrometer and a 25 mCi ^{57}Co source in a Rh matrix. The velocity scale was calibrated using α-Fe foil. Isomer shifts are given relative to metallic α-Fe at 300 K. The disk-shaped absorber was obtained by gently packing the sample single crystals into a Perspex holder. Low temperature spectra were collected using a liquid helium JANIS bath cryostat with the sample in He exchange gas or, for measurements at 4 K, immersed in liquid He. The spectra were fitted to Lorentzian lines using a non-linear least-squares method.[20]

Magnetic measurements

Magnetic measurements were performed in a S700X SQUID magnetometer with a 70 kG magnet (Cryogenic Ltd.) using polycrystalline samples. The temperature dependence of the magnetic susceptibility in the temperature range 2–320 K was measured under a magnetic field of 10 kG. For measurements with temperatures higher than 320 K a 55 kG MPMS SQUID magnetometer (Quantum Design) was used. A Maglab 2000 system (Oxford Instruments) was used for ac susceptibility measurements down to 1.5 K, in the frequency range 99–9990 Hz, with 1 G ac field. The paramagnetic susceptibility was obtained from the experimental magnetization (assuming that $\chi = M/H$) data after a diamagnetism correction was estimated from tabulated Pascal constants.

Conclusions

In this article we report the synthesis and the structural and magnetic characterization of the new hybrid molecular magnet $[Fe(5\text{–}Cl\text{-}qsal)_2][Ni(\alpha\text{-}tpdt)_2]$ CH_3CN (**1**), displaying a SCO transition at room temperature ($T_{1/2} = 298$ K) and a FM cluster-glass behavior at low temperatures ($T_b = 7.5$ K). The magnetic behavior of this hybrid material results from the intermolecular arrangements in the crystal structure, consisting in segregated layers of $[Fe(5\text{–}Cl\text{-}qsal)_2]^+$ cations and $[Ni(\alpha\text{-}tpdt)_2]^-$ anions. At both RT and 150 K, a detailed crystal structure analysis shows the existence of a segregated cationic–anionic layer structure, where both layers are based on arrangements of cationic or anionic chains.

The SCO behavior, probed by ^{57}Fe Mössbauer spectroscopy and the magnetic susceptibility temperature dependence, is associated with the cationic layer. Although the spin conversion is well defined at $T_{1/2} = 298$ K, this phenomena spreads from low temperatures (~30 K) up to more than 400 K. The rather sluggish completion of the transition for the limits of the spin conversion is attributed to relative stiffness of the anionic network and solvent molecules surrounding the cations.

The analysis of the intermolecular coupling in the anionic layers through the McConnell I mechanism suggests the coexistence of sizable intrachain FM interactions with weaker AF intrachain interactions, which is in good agreement with the low temperature magnetic susceptibility, where most of the Fe^{III} atoms are in the LS state. Below *ca.* 7.5 K a FM cluster-glass behavior was observed and characterized by dc magnetization and ac susceptibility studies. This behavior is attributed to the formation of small FM 2D domains with cooling, with weak AF interdomain interactions.

The hybrid behavior of **1** is also supported by the Mössbauer studies that show no sign of intermediate or slow relaxation of the Fe^{III} magnetic moments in the ^{57}Fe Mössbauer spectrum at 4 K. The observation of quadrupole doublets with narrow peaks at 4 K evidences a relaxation frequency of the Fe moments higher than 10^8 s^{-1}, typical of paramagnetic behavior.

Acknowledgements

This work was partially supported by Fundação para a Ciência e Tecnologia (Portugal) under contracts PDCT/QUI/64967/2006, PTDC/QUI/65379/2006. This work also benefited from COST action D35 and MAGMANet network of excellence.

References

1 For a general overview see P. Gütlich and H. A. Goodwin, *Top. Curr. Chem.*, 2004, **233**.
2 For a general overview see A. B. Gaspar, V. Ksenofontov, M. Seredyuk and P. Gütlich, *Coord. Chem. Rev.*, 2005, **249**, 2661–2676.
3 (*a*) D. Belo, H. Alves, S. Rabaça, L. C. Pereira, M. T. Duarte, V. Gama, R. T. Henriques, M. Almeida, E. Ribera, C. Rovira and J. Veciana, *Eur. J. Inorg. Chem.*, 2001, 3127–3133; (*b*) J. P. M. Nunes, M. J. Figueira, D. Belo, I. C. Santos, B. Ribeiro, E. B. Lopes, R. T. Henriques, C. Rovira and M. Almeida, *Chem.–Eur. J.*, 2007, **13**, 9841; (*c*) D. Belo, H. Alves, E. B. Lopes, M. T. Duarte, V. Gama, R. T. Henriques, M. Almeida, A. Pérez-Benítez, C. Rovira and J. Veciana, *Chem.–Eur. J.*, 2001, **7**, 511–519; (*d*) D. Belo, M. J. Figueira, J. Mendonça, I. C. Santos, M. Almeida, R. T. Henriques, M. T. Duarte, C. Rovira and J. Veciana, *Eur. J. Inorg. Chem.*, 2005, 3337–3345.
4 (*a*) D. Belo, J. Mendonça, I. C. Santos, L. C. J. Pereira, M. Almeida, J. J. Novoa, C. Rovira, J. Veciana and V. Gama, *Eur. J. Inorg. Chem.*, 2008, 5327–5337; (*b*) D. Belo, M. J. Figueira, J. P. M. Nunes, I. C. Santos, L. C. Pereira, V. Gama, M. Almeida and C. Rovira, *J. Mater. Chem.*, 2006, **16**, 2746–2756; (*c*) D. Belo, L. C. J. Pereira, M. Almeida, C. Rovira, J. Veciana and V. Gama, *Dalton Trans.*, 2009, 4176–4180.
5 (*a*) K. Takahashi, H.-B. Cui, Y. Okano, H. Kobayashi, H. Mori, H. Tajima, Y. Einaga and O. Sato, *J. Am. Chem. Soc.*, 2008, **130**, 6688–6689; (*b*) K. Takahashi, H.-B. Cui, H. Kobayashi, Y. Einaga and O. Sato, *Chem. Lett.*, 2005, **34**, 1240–1241; (*c*) K. Takahashi, H.-B. Cui, Y. Okano, H. Kobayashi, Y. Einaga and O. Sato, *Inorg. Chem.*, 2006, **45**, 5739–5741; (*d*) S. Hayami, T. Kawahara, G. Juhasz, K. Kawamura, K. Uehashi, O. Sato and Y. Maeda, *J. Rad. Nucl. Chem.*, 2003, **255**, 443–447; (*e*) S. Hayami, Z. Gu, H. Yoshiki, A. Fujishima and O. Sato, *J. Am. Chem. Soc.*, 2001, **123**, 11644–11650; (*f*) J. C. Dias, B. J. C. Vieira, I. C. Santos, L. C. J. Pereira and V. Gama, *Inorg. Chim. Acta*, 2009, **362**, 2076–2079.
6 M. Clemente-León, E. Coronado, M. C. Giménez-López, A. Soriano-Portillo, J. C. Waerenborgh, F. S. Delgado and C. Ruiz-Pérez, *Inorg. Chem.*, 2008, **47**, 9111–9120.
7 H. M. McConnell, *J. Chem. Phys.*, 1963, **39**, 1916.
8 J. A. Mydosh*"Spin Glasses: An Experimental Introduction"*, Taylor & Francis, London1993.
9 B. Antic, G. F. Goya, H. R. Rechenberg, V. Kusigerski, N. Jovic and M. Mitric, *J. Phys.: Condens. Matter*, 2004, **16**, 651.
10 R. N. Bhowmik and R. Ranganathan, *J. Magn. Magn. Mater.*, 2002, **248**, 101.
11 (*a*) K. Mukherjee and A. Banerjee, *Phys. Rev. B: Condens. Matter Mater. Phys.*, 2008, **77**, 024430-1–9; (*b*) K. De, M. Patra, S. Majumdar and S. Giri, *J. Phys. D: Appl. Phys.*, 2007, **40**, 7614–7619; (*c*) D. N. H. Nam, K. Jonason, P. Nordblad, N. V. Khiem and N. X. Phuc, *Phys. Rev. B: Condens. Matter Mater. Phys.*, 1999, **59**, 4189–4194; (*d*) D. X. Li, S. Nimori, Y. Shiokawa, Y. Haga, E. Yamamoto and Y. Onuki, *Phys. Rev. B: Condens. Matter Mater. Phys.*, 2003, **68**, 172405-1–4; (*e*) S. Sério, L. C. J. Pereira, M. M. Cruz, A. Godinho and J. C. Waerenborgh, *J. Alloys Compd.*, 2008, **454**, 16–23.

12 J. C. Dias, J. C. Nunes, B. Vieira, I. C. Santos, L. C. J. Pereira, J. C. Waerenborgh, V. Gama, to be published.
13 G. M. Sheldrick, *SADABS*, Bruker AXS Inc., Madison, Wisconsin, USA, 2004.
14 Bruker SMART and SAINT, Bruker AXS Inc., Madison, Wisconsin, USA, 2004.
15 A. Altomare, M. C. Burla, M. Camalli, G. Cascarano, G. Giacovazzo, A. Guagliardi, A. G. G. Moliterni, G. Polidori and R. Spagna, *J. Appl. Crystallogr.*, 1999, **32**, 115.
16 G. M. Sheldrick, *SHELXL97, Program for Crystal Structure Refinement*, University of Göttingen, Germany, 1997.
17 L. J. Farrugia, *J. Appl. Crystallogr.*, 1999, **32**, 837.
18 L. J. Farrugia, *J. Appl. Crystallogr.*, 1997, **30**, 565.
19 G. Nolze, W. Krauss, *PowderCell 2.3 program*, BAM berlin, 2000.
20 J. V. Rodrigues, I. C. Santos, V. Gama, R. T. Henriques, J. C. Waerenborgh, M. T. Duarte and M. Almeida, *J. Chem. Soc., Dalton Trans.*, 1994, 2655.

